applied sciences

MDPI

Review

Frequency Comb-Based WDM Transmission Systems Enabling Joint Signal Processing

Lars Lundberg *, Magnus Karlsson, Abel Lorences-Riesgo †, Mikael Mazur, Victor Torres-Company and Jochen Schröder and Peter A. Andrekson

Department of Microtechnology and Nanoscience, Chalmers University of Technology, SE-412 96 Göteborg, Sweden; magnus.karlsson@chalmers.se (M.K.); abellorences@av.it.pt (A.L.-R.); mikael.mazur@chalmers.se (M.M.); torresv@chalmers.se (V.T.-C.); jochen.schroeder@chalmers.se (J.S.); peter.andrekson@chalmers.se (P.A.A.)

* Correspondence: lars.lundberg@chalmers.se

† Current address: IT-Instituto de Telecomunicações, 3810-193 Aveiro, Portugal.

Received: 31 March 2018; Accepted: 27 April 2018; Published: 4 May 2018

Abstract: We review the use of optical frequency combs in wavelength-division multiplexed (WDM) fiber optic communication systems. In particular, we focus on the unique possibilities that are opened up by the stability of the comb-line spacing and the phase coherence between the lines. We give an overview of different techniques for the generation of optical frequency combs and review their use in WDM systems. We discuss the benefits of the stable line spacing of frequency combs for creating densely-packed optical superchannels with high spectral efficiency. Additionally, we discuss practical considerations when implementing frequency-comb-based transmitters. Furthermore, we describe several techniques for comb-based superchannel receivers that enables the phase coherence between the lines to be used to simplify or increase the performance of the digital carrier recovery. The first set of receiver techniques is based on comb-regeneration from optical pilot tones, enabling low-overhead self-homodyne detection. The second set of techniques takes advantage of the phase coherence by sharing phase information between the channels through joint digital signal processing (DSP) schemes. This enables a lower DSP complexity or a higher phase-noise tolerance.

Keywords: optical frequency comb; fiber optic communication; coherent detection; digital signal processing (DSP); carrier recovery

1. Introduction

The advent of the erbium-doped fiber amplifier (EDFA) in the late 1980s [1,2] transformed fiber optic communications in two profound ways. The first was that it enabled radically increased link distances without resorting to electrical regeneration. The second and equally profound impact was that it facilitated wavelength-division multiplexing (WDM), i.e., the transmission of data on many parallel laser carriers of different wavelengths. The first demonstrations of amplified WDM data transmission came in 1990 [3,4] and were followed by massive commercial installations of WDM systems during the second half of the 1990s [5]. These developments paved the way for affordable worldwide telecommunications, and more specifically, the Internet, as we know it today. Current optical WDM systems and state-of-the-art experiments demonstrating transmission records may use hundreds of wavelengths in a single fiber core [6], requiring large stacks of lasers in the transmitters. In addition, the increased popularity of coherent intradyne links [7,8] with receivers needing local oscillator lasers and digital signal processing (DSP) have highlighted the need for coherent sources also in the receiver.

The question that arises is if a frequency comb, comprising a large number of phase-locked spectral lines, could be a viable alternative as WDM sources and replace discrete laser stacks. The answer is yes, although some care needs to be taken to ensure source figure of merits such as the line width and signal-to-noise ratio (SNR) are met. In this paper we will review the work on using optical frequency combs for WDM transmission and put particular emphasis on discussing the unique benefits that are enabled by the use of frequency combs in contrast to discrete lasers.

This introduction will continue with a history of optical frequency combs and their use in WDM systems. Then, we will briefly outline the unique possibilities that combs enable in optical communications, as well as provide an overview for the remaining sections of this article.

1.1. Optical Frequency Combs: A Background

An optical frequency comb is a set of evenly-spaced lines in the frequency domain, f_n, whose location is given by $f_n = nf_r + f_0$, illustrated in Figure 1. In the time domain, this corresponds to a train of optical pulses. In the expression above, f_r defines the line spacing, which relates to the inverse of the period in the pulse train (repetition rate). Note that the frequency lines are offset from zero by the quantity f_0. This offset indicates that the oscillation frequencies of the spectral lines are not necessarily a multiple integer of the repetition rate. Since the offset frequency f_0 is in the most general case independent of f_r, there are two degrees of freedom in an optical pulse train that define the absolute position of the lines in the frequency domain.

The origin of the offset frequency depends on the specific comb generation technology used. For mode-locked lasers, it depends on the relation between the group and phase velocity in the resonating cavity, while for combs generated as modulation spectra around a central frequency f_c, it depends on the absolute value of this central frequency. Here, it should be noted that for the latter kind of frequency combs, f_c is often used instead of f_0 to define the absolute position of the comb. This definition is also commonly used in telecom applications.

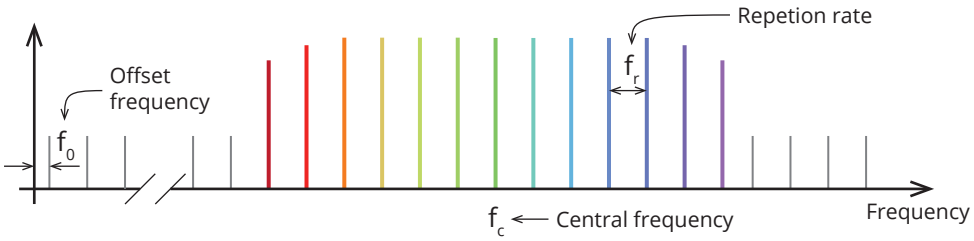

Figure 1. A frequency comb in the frequency domain. The comb is fully characterized by the repetition rate f_r, which defines the line spacing, and either the offset frequency from zero f_0 or the central frequency f_c.

1.1.1. Technologies for Optical Frequency Comb Generation

There is a vast range of laser technologies that qualifies as optical frequency comb generators. Each has different tradeoffs and can be engineered to meet different application-specific requirements. The first optical comb generators were based on the electro-optic modulation method [9,10], often known as electro-optic frequency comb generators or simply electro-optic (EO) combs. In its most basic configuration, a continuous-wave (CW) laser is modulated by an electro-optic modulator. The modulator is itself driven by an external radio-frequency (RF) source. The modulation creates sidebands around the CW laser exactly spaced by the frequency of the RF source. Here, the frequency of the CW laser and the frequency of the RF source provide the two degrees of freedom of the comb generator. One common setup for an EO-comb is illustrated in Figure 2.

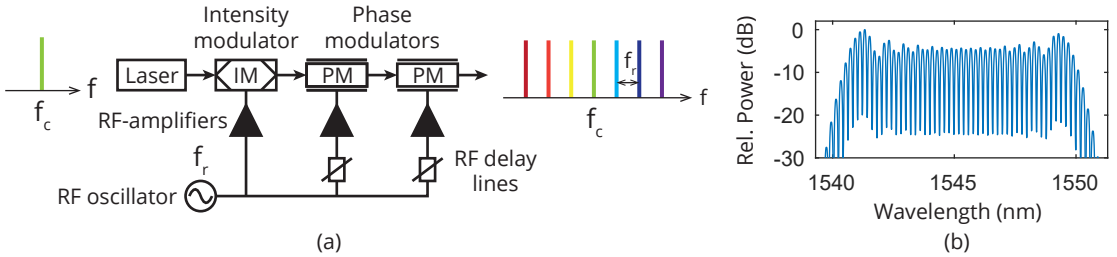

Figure 2. (**a**) A common setup of an electro-optic (EO) comb. A radio-frequency (RF) oscillator with frequency f_r is used to phase- and intensity-modulate a continuous-wave laser, which creates an optical frequency comb with central frequency f_c and frequency spacing f_r. The RF delay lines are adjusted so that the intensity modulator carves out the part of the light where the phase modulation is mostly linear, which enables a relatively flat comb. Several phase modulators can be used to increase the modulation depth without increasing the RF input power to the modulators, which increases the total number of comb lines. (**b**) Measured spectrum of an EO-comb.

EO combs built with state-of-the-art, yet standard, telecommunication equipment feature high average power (∼1–10 mW per line), a low optical linewidth (<100 kHz) and a smooth optical envelope [11,12]. The RF source can be derived from high-performance RF oscillators, which translates into optical pulse trains with low timing jitter [13].

During the 1990s, there was a rapid development of ultrafast solid state mode-locked laser technology [14] and efficient nonlinear broadening mechanisms in photonic crystal fibers [15]. By the end of the decade, it became possible to implement the concept of self-referencing, whereby the two degrees of freedom of the comb could be locked to a common radio-frequency reference [16,17].

However, modern light wave communications do not need combs with the frequency lines defined with such a level of accuracy. Instead, the lines need to display a high optical signal-to-noise ratio (OSNR) (>30 dB), a spacing in the order of 10–100 GHz, optical linewidths <100 kHz, a smooth spectral envelope and compatibility with fiber-optic components (ideally in a small and robust form factor). These demands, especially the line spacing, have challenged the use of more standard frequency comb generators used in frequency metrology applications, such as those based on erbium fiber mode-locked lasers, for applications in optical communications.

Using combs as alternatives to discrete laser sources was explored based on nonlinearly broadened (so-called supercontinuum) pulses from mode-locked fiber lasers already in 1996 [18]. While enabling transmission records, those sources where not strict comb sources as the comb line separation was much smaller than the channel separation, and optical time-division multiplex filters were needed to increase the symbol rates. However, a few years later, it was recognized that optical frequency combs, particularly those based on EO comb technology, could be very attractive as WDM sources. This concept was originally explored with nonlinear broadened EO combs using on-off keying in [19]. The initial demonstrations involved a limited number of channels, but subsequent progress in highly nonlinear fibers enabled extending the concept to >1000 lines [20].

The aforementioned EO combs represent an excellent choice for exploring the possibilities of frequency combs as sources in WDM systems. The time-domain waveform emerging from an EO comb can be compressed to generate picosecond pulses [10], which can be used as the seed to generate additional bandwidth via nonlinear effects in an external waveguide (see, e.g., [21,22]). By carefully shaping the pulses and the dispersion in the nonlinear medium, combs spanning the C + L light wave communication bands with high OSNR can be obtained [23].

The introduction of coherent technology in WDM systems imposed additional demands on the optical linewidth and OSNR for the comb lines. During the last five years, there has been a remarkable progress in nonlinearly broadened EO combs [23–25]. This type of comb has been used as a WDM source and enabled complex modulation formats in single-core [26,27] and multi-core fiber systems [28]. The latter results are remarkable because they illustrate that a comb source derived from a single seed

CW laser has sufficient OSNR performance to light multiple frequency channels simultaneously in multiple spatial modes.

1.1.2. Integration Potential of Frequency Combs

WDM communications with frequency combs naturally entail multiple frequency channels. Unless thermal management becomes an insurmountable obstacle, it is desirable to work with combs integrated on the same chip as the other necessary components to build a WDM transmitter/receiver. This has motivated research into alternative chip-scale comb platforms. Semiconductor-based mode-locked lasers allow for co-integrating the gain section and saturable absorber on the same chip and attain a very short cavity round trip time to allow for fundamental mode locking at repetition rates approaching 100 GHz. In two-section semiconductor-based mode-locked lasers, the repetition rate is given by the free spectral range of the cavity, and the carrier offset frequency can be independently controlled by finely tuning the injection current [29]. Semiconductor quantum dots allow for broadband gain and an ultrafast carrier recovery time, leading to sub-picosecond pulse formation in a compact platform [30]. Unfortunately, the carrier dynamics leads to increased absorption losses, resulting in an increased optical linewidth of the modes and timing jitter. Research efforts are ongoing towards devising external cavity lasers to reduce the modal instability [31]. This motivates the research behind hybrid III-V-on silicon technology, since silicon waveguides can provide lower losses [32,33].

An alternative strategy to reach a high-level of stability in repetition rate is to perform hybrid mode locking in dual-section semiconductor mode-locked lasers, i.e., modulating the saturable absorber with an external RF commensurate to the free spectral range of the cavity. This notwithstanding, good results in the context of WDM communications can be realized with single-section passively mode-locked quantum dot InAs/InP lasers [34]. These lasers feature optical linewidth in the ∼10 MHz range, but the instantaneous linewidth is much narrower, thus enabling complex modulation formats [35]. Recent results indicate that self-injection locking with the aid of an external (free space) cavity can lead to a dramatic decrease in both optical linewidth and timing jitter [36].

Gain-switched laser diodes provide an interesting alternative as an integrated comb generator because they are very power efficient [37]. Reduction of the optical linewidth can be attained by injection locking to a master laser oscillator [38]. One additional challenge with this platform is scaling up the bandwidth and repetition rate to frequencies going significantly beyond 10 GHz.

Another comb source that is promising for WDM applications is a microresonator frequency comb [39]. Here, a CW laser pumps a longitudinal mode of an integrated nonlinear cavity. The third-order nonlinearity generates new frequency components via four-wave-mixing. The first experiments were done in whispering gallery mode resonators [40], but comb generators based on high-Q silicon nitride technology [41] have been demonstrated by several laboratories around the world [42–46]. This material platform is interesting for WDM communications because it is based on silicon photonics technology, which means that the devices can be grown on silicon wafers and complementary metal-oxide-semiconductor (CMOS) fabrication techniques can be used. This allows for leveraging the well-established CMOS processes to decrease the price of large volume processing.

Soon after the first demonstrations of silicon nitride microresonator combs, it became clear that the technology could be used as the WDM source [47–50]. In particular, temporal cavity solitons (or dissipative Kerr solitons) are short pulses of light circulating in the cavity that balance the dispersion broadening with a nonlinear phase shift and compensate for the inherent absorption losses with parametric gain [51]. The bell-shaped characteristic of the pulses in the time domain translates into a comb of frequencies with a very smooth envelope. Recent demonstrations indicate that these combs can be precisely engineered to cover the light wave communications C + L bands [52]. The performance in terms of optical linewidth and OSNR is sufficiently high to encode high-baud rate complex modulation formats [52,53]. A fundamental challenge with temporal cavity solitons is that the conversion efficiency from the CW laser to total comb power is inversely proportional to the number of generated comb lines [54]. This means that the power of the individual lines is inversely

proportional to the square of the number of comb lines, and a high-power CW laser is needed to achieve the target OSNR.

Alternatively, mode-locked dark-pulse combs, as recently demonstrated in silicon nitride microresonators [55], display much higher conversion efficiency [56]. These comb sources have enabled complex modulation formats while keeping a CW pump power of 100 mW [57]. One drawback of this comb is that the spectral envelope is not as smooth as with temporal cavity solitons. It is still unclear which of these two sources provides a better solution as the WDM source. Other open research questions relevant for coherent communications using microresonator frequency comb technology are the line spacing stability [58–60] and hybrid integration.

A main motivation for using frequency combs as WDM sources is the potential of reducing hardware complexity and power consumption by replacing a large amount of individual laser sources, each of which needs individual thermal control and other control circuits. In the Supplementary Material of [52], the power consumption of microresonator combs is compared to that of discrete lasers and found to be lower if a sufficient number of lines is generated (the exact number depends on the specific comb design). Apart from this, the power consumption of comb generation has not been well studied.

1.2. Unique Comb Benefits

Beside potential gains in terms of reduced hardware complexity and power consumption, there are also other, transmission- and signal quality-related gains to be had from the use of combs. The central difference of using a comb instead of separate lasers is that the comb lines are essentially phase-locked to each other, which is illustrated by the expression for the electric field of a comb [61]:

$$E(t) = \sum_n E_n \exp[-i2\pi f_n t + \phi(t) + 2\pi n f_r \Delta T(t)]. \quad (1)$$

Here, $f_n = nf_r + f_0$ are the frequency comb lines, with fixed complex amplitude, E_n. The random functions $\phi(t)$ and $\Delta T(t)$ represent the phase and timing jitter noise in the comb. If the timing jitter of the comb can be controlled (that is, it can be ignored for all practical purposes), the phase noise is correlated among the comb lines. Such a broadband phase coherence constitutes a key resource in many metrology applications of frequency combs [62], but this aspect has hitherto been ignored in most WDM systems where the channels are measured on an individual basis. Controlling the timing jitter is not always straightforward. However, the above equation also shows that the phase noise only depends on two random functions. This leads to the important property that the phase noise of all comb lines can be characterized by measuring the phase fluctuations of only two lines.

In this paper, we will discuss how the stability in repetition rate and broadband phase coherence of frequency combs can be exploited in the design and operation of coherent WDM systems. The paper partly summarizes our work in [63–68] and puts it into a broader context. Specifically, we focus on techniques for utilizing the phase coherence to relieve the digital carrier recovery in the receiver. In addition to reviewing previous work, we also present some previously unpublished results.

The following unique features of optical frequency combs will be discussed:

- They enable the WDM channels to be more densely packed, requiring smaller guard bands between the channels, since they drift in frequency in a correlated manner, in contrast to separate laser sources. Such comb-based superchannels will be discussed in Section 2.
- They enable optical pilot signals that can be co-transmitted with the data with unprecedented low overhead, since two pilots are sufficient to regenerate a local-oscillator comb phase-locked to the transmitter comb for 50 WDM channels or more. Such pilot-based comb regeneration will be discussed in Section 3.
- They enable joint digital signal processing with reduced complexity or increased phase-noise tolerance, since the retrieved phase from one channel can be reused for the other channels or

used to increase the SNR of the phase estimate. Such joint signal processing algorithms will be discussed in Section 4.

In addition, comb-based transmission enables other benefits that can be useful in WDM transmission, but will not be discussed in depth here. A notable example is the use of coherent combs for sub-band detection of high-bandwidth signals, for which electrical oscilloscopes cannot capture all features. Such metrology aspects have been explored by Fontaine et al. [69]. This technique can also be utilized to measure wideband optical data signals [70]. Furthermore, in digital predistortion experiments to compensate for nonlinear WDM impairments, comb sources are needed to ensure frequency stability between channels [71,72].

This review is organized as follows: Section 2 is devoted to comb-based superchannels and their transmitter considerations, and Section 3 deals with the use of combs in receivers and regeneration of combs from optical pilots. Section 4 deals with joint receiver algorithms, i.e., sharing phase information between channels in DSP. Finally, in Section 4, we conclude this paper.

2. Comb-Based Superchannels

A superchannel [73] is in the most broad sense a set of channels that is considered one entity, so that all subchannels are transmitted, routed and received together. Due to this, the channels can be spaced densely and guard bands, required to allow for individual routing of channels in an optical network, can be avoided. The concept was first proposed to allow increasing the channel bandwidth beyond what is possible on a single optical carrier due to limited bandwidth of electrical components. Since then, the concept has expanded to cover every aspect of multiple jointly-treated channels. The subchannels can be separated into either the spatial [74] or the spectral domain [75]. This section will discuss the challenges and benefits brought by using frequency combs to realize superchannels.

Superchannels constructed by combining several densely-spaced wavelength carriers are required to reach target line rates approaching 1–10 Tb/s, needed to support next generation router interfaces [74]. Even looking beyond state-of-the-art electrical and optical hardware supporting bandwidths up to and beyond 100 GHz enabling demonstrations of 180-Gbaud quadrature phase-shift-keying (QPSK) transmission [76], the required electrical bandwidth is significantly beyond what can be achieved using a single wavelength carrier. Considering state-of-the-art integrated transceivers capable of transmitting symbol rates up to 100 Gbaud [77] and assuming that such a transceiver could reach the current record WDM spectral-efficiency of 14.2 bits/4D-symbol reported in [78], about seven transceivers are still required to reach the 10-Tb/s line rate. Following this, it is important to note that even though a superchannel consists of several subchannels, each subchannel needs to have as high throughput as possible to avoid loss in spectral efficiency.

2.1. Superchannel Transmitter Requirements

In this subsection, we will discuss the requirements of comb-based versus discrete laser array-based light sources for superchannel generation. We first focus on how the required OSNR (OSNR refers to the noise power within a bandwidth of 0.1 nm throughout this paper) translates into varying comb requirements. This is followed by a discussion on inter-channel guard bands and the role of frequency combs in enabling ultra-dense WDM.

2.1.1. OSNR Requirements

For comb-based superchannels, the key assumption is that the underlying comb source can provide the required line power to reach sufficient OSNR at the transmitter side. This can be analyzed by comparing a comb-based transmitter to a transmitter using a laser array, as illustrated in Figure 3. In the case of a laser array, each laser is directly connected to the modulators, and assuming equal line power is therefore natural. This is the classical system and will be our benchmark. A multi-wavelength comb source cannot, generally, beat the OSNR of a free-running laser since practical power limitations

will always degrade the maximum line power. The required input power to the modulator to reach a certain transmitter side OSNR is:

$$P_{\text{Mod}} = \text{OSNR}_{\text{TX}} + \text{NF}_{\text{EDFA}} + \text{IL}_{\text{Mod}} - 58\,\text{dBm}, \tag{2}$$

where OSNR_{TX} is the desired transmitter side OSNR, NF_{EDFA} the noise figure of the post-mux EDFA in Figure 3 and IL_{Mod} the overall loss of the modulation stage. The -58 dBm is the vacuum fluctuation-limited, dual-polarization noise power (The value -58 dBm can be calculated from $h\nu_0\Delta\nu_0$, where h is the Planck constant, ν_0 is the frequency of the carrier and $\Delta\nu$ is the noise bandwidth, corresponding to 0.1 nm. More details can be found in e.g., [79]). When free-running lasers are used, P_{Mod} is the required output power needed. In the case of comb-based transmission, the losses of the comb generation stage need to be taken into account to calculate the output power of the comb seed laser, P_{Comb}. Assuming a comb generator without amplification, the input power to the comb generation stage is then:

$$P_{\text{Comb}} = P_{\text{Mod}} + 10 \cdot \log_{10}(N) + \text{IL}_{\text{Comb}} + P_{\text{Line Diff.}}, \tag{3}$$

where $10 \cdot \log_{10}(N)$ represents the number of lines among which the power is divided, IL_{Comb} the insertion loss of the comb regeneration stage and $P_{\text{Line Diff.}}$ the difference between average and minimum line power.

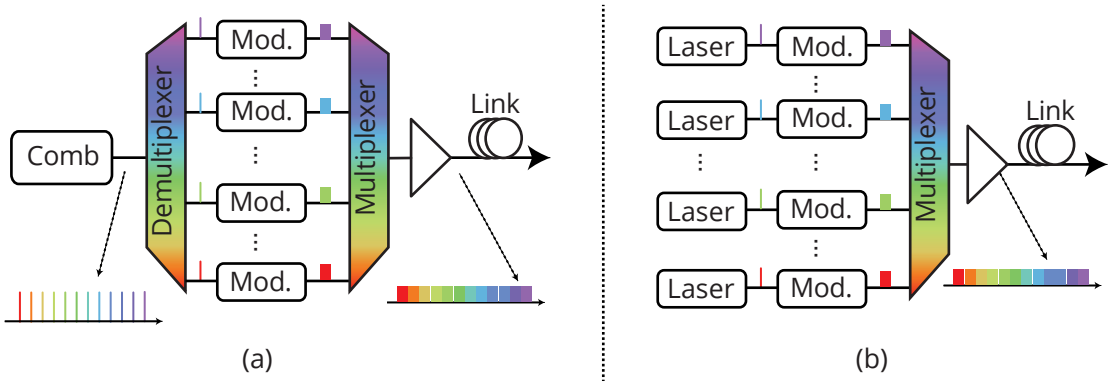

Figure 3. Schematic of (**a**) a comb-based transmitter and (**b**) a transmitter using a laser array. Mod.: Modulator.

As a simple comparison point, assume that the post-mux EDFA has a noise figure of 5 dB and the required OSNR is 30 dB. The loss for modulating the high spectral-efficiency signal including the multiplexer to combine all signals prior to amplification into the span is around 15 dB. The required output power for each laser in a laser array is then -8 dBm.

Assuming that a comb is used to generate these lines, the required power grows fast with the number of lines. Considering the case of a 50-line loss-free comb source and a perfect flat envelope without excess lines ($N = 50, \text{IL}_{\text{Comb}} = 0, P_{\text{Line Diff.}} = 0$), only the power division between the lines needs to be considered. The input power to the comb then has to be 9 dBm, which is clearly reachable using a non-amplified pump line. In practice, however, combs are neither loss-free, nor spectrally flat or without any excess lines. Considering the case of a 50-line EO-comb with the spectral flatness $P_{\text{Line Diff.}}$ of about 6 dB and total insertion loss of 12 dB [67], the required input power is 27 dBm. While this is easily reachable using high-power amplifiers, one would ideally like to avoid such components and have the laser directly connected to the comb source. Depending on the technology used, these values can vary, but they still show the challenge in designing comb-based transmitters for multiple lines and high OSNRs. Moreover, depending on the comb-technology used, tuning the number of lines, as well

as the flattening can be very difficult. However, a 10-line superchannel would require a pumping power of 20 dBm, which is feasible with integrated laser technology [80].

While it can be challenging to support high line counts, it is also important to discuss these requirements from a broader perspective. Key considerations are then the maximum available comb seed power and the comb flatness. In the example above, we assume that all lines are modulated with the same format and the performance is simply dictated by the worst performing channel. By using adaptive-rate forward error correction (FEC) , constellation shaping or similar techniques, the required flatness could likely be relaxed. Similarly, the challenge of maintaining high OSNR in transmission is likely to affect the number of lines included in each superchannel. While a single comb-source spanning the full C-band might be a clear target, spectral flatness combined with the simple line multiplication factor could make such implementations less attractive.

2.1.2. Guard Bands

While the bandwidth of electronics is increasing rapidly, several Tb/s line rates are not feasible using a single wavelength channel, and thus, multiplexing is required [81]. In such scenarios, dense packing is required to avoid the loss of spectral efficiency due to inter-channel guard bands [75]. This is a promising use case for frequency combs as the phase-locked carriers avoid channel drifts and allow for dense packing beyond what can be achieved using free-running lasers. This can be fully utilized in coherent superchannels, since the subchannels are routed together, and no guard bands are needed to account for the limited granularity of wavelength demultiplexers.

The advantage of combs can be seen by considering a required guard band of 1 GHz in the case of free-running lasers. For a 100-Gbaud channel, this results in 1% loss of spectral efficiency. Considering slicing this channel into 10 subcarriers using free-running lasers, the equivalent guard-band penalty is then 10% of the channel width. However, if frequency combs are employed, the required guard bands can be as low as 100 MHz [82], again resulting in an equivalent guard-band penalty of 1% of the channel width. Thus, a comb-based superchannel using 100×10 Gbaud channels and a system using free-running lasers and 10×100 Gbaud have an equivalent guard-band overhead. This can be exploited to ease the requirements for very high spectral efficiency transmission as the effective number of bits (ENOBs) usually is highly limited at high symbol rates [81]. At the expense of employing additional transmitters, combs can therefore enable higher spectral efficiency by simply allowing for forming a superchannel containing more lower-symbol rate channels.

3. Receiver Comb Technologies

In coherent WDM systems, a local oscillator (LO) laser in the receiver is needed for data detection of each carrier, and the most straightforward scheme is independent LO lasers for every channel. An obvious question is then if and why one would like to use a comb for the local oscillators. Aside from potential (though yet to be verified in the scientific literature) gains in power dissipation and complexity, can comb-based local oscillators provide any benefits from a transmission performance perspective? The answer is yes, but only provided phase-locked (hence comb-based) carriers are used in the transmitter side. Then, phase-locked LOs will preserve the phase-locking of the channels also after detection, which would otherwise be broken by the independent phase-noise of the LOs. We note that a single LO laser can also be used to detect a superchannel in a very broadband receiver, while preserving the phase-locking of the channels [82,83], but will ultimately be limited by the bandwidth of photodetectors and analog-to-digital converters (ADCs).

We will discuss two approaches for comb-based receivers that utilize the phase-locking of the channels in this paper (see Figure 4). The first approach is to regenerate the transmitter comb and use it as the LO, which is discussed later in this section. The second approach is to use separate free-running combs in the transmitter and receiver and then to use joint digital signal processing (DSP) between the channels. This approach is discussed in Section 4 below.

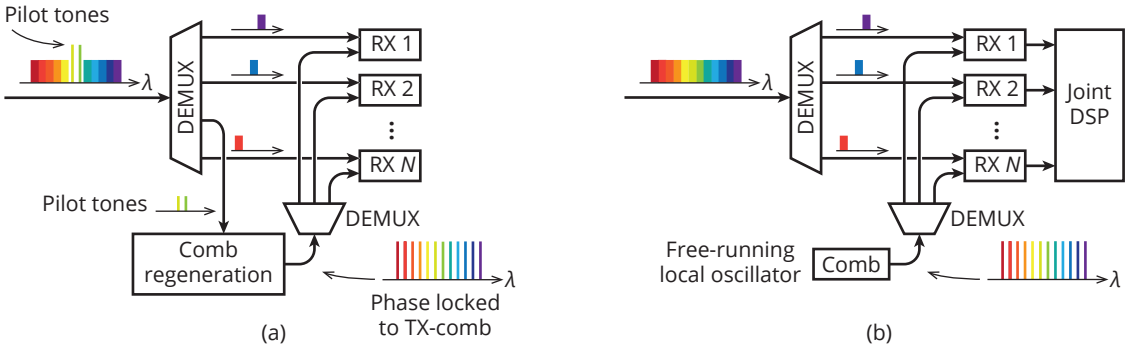

Figure 4. Schematic of two different comb-based receiver principles. (**a**) Comb regeneration based on two pilot tones. Since the local-oscillator (LO) comb is phase-locked to the transmitter comb, the receiver digital signal processing (DSP) can be simplified. (**b**) Unsynchronized local oscillator comb and joint DSP. RX: Receiver.

3.1. Exploiting Subchannel Phase Coherence

The frequency-locked and phase coherent properties of subchannels can be exploited to either completely replace or increase the efficiency of the DSP carrier recovery in the receiver. In a phase noise limited system, this can be utilized to increase performance. Additionally, even if performance is not limited by phase noise, eliminating or simplifying the carrier recovery leads to a reduction in DSP complexity and power consumption. This is particularly interesting for short-reach links using higher-order modulation formats, whose higher phase-noise sensitivity increases the complexity of the carrier recovery. In addition, shorter links need to spend less power on the dispersion compensation, making the carrier recovery a proportionally bigger part of the DSP power consumption.

In this context, connections between comb-based systems and systems employing space-division multiplexing (SDM) can be made. For SDM, using the same laser for several channels transmitted over different cores/modes in an SDM fiber leads to these spatial channels sharing the same frequency and the same phase noise. Similarly, all spectral channels originating from an optical frequency comb mostly share the same phase noise. However, while the scenarios are very similar, the two are not identical. As discussed in Section 1, frequency combs are inherently characterized by two frequencies, the central frequency and the line spacing, and in general, there will be phase noise differences between the lines.

The methods for exploiting subchannel coherence can be roughly divided into two categories, pilot tone based or methods based on joint carrier recovery in DSP. The pilot tone-based methods work by multiplexing one or several pilot tones extracted directly from the carrier light source with the superchannel. The carrier phase can then be extracted from the pilot tones in the receiver. In contrast, joint carrier-recovery methods extract the carrier phase information using DSP on the data channels, further discussed in Section 4.

The phase information carried in pilot tones can be extracted or detected in the receiver using several different methods, which can be divided into optical and electrical/digital methods. In the optical approach, the pilot tones are used (directly or with additional analog processing) to create LOs that are phase-locked to the carriers, causing the downconverted signals to be (ideally) without carrier offset. These methods are commonly known as self-homodyne methods [84]. Self-homodyne methods can enable coherent transmission using high-linewidth light sources [85], as well as savings in DSP complexity [86].

The amount of processing of the pilot tones needed for self-homodyne detection differs depending on the system type. In SDM systems, processing is usually limited to amplification and filtering of the pilot tones, while comb-based superchannels need to regenerate a full comb from co-transmitted pilot tones. Such comb regeneration can be done in several ways and will be discussed below in Sections 3.2–3.4.

For the electrical/digital approach, the pilot tones are detected jointly with the signals using a separate (free-running) LO, and then, the relative phase between pilot and signal is extracted in DSP. This is known as digital self-homodyne detection [87] or shared-carrier reception [88].

3.2. Regeneration from Two Pilots

As stated in Equation (1), the phase evolution of each comb carrier can be written in terms of the phase and timing-jitter noise. Thus, by knowing the phase evolution of two carriers, the phase evolution of any carrier can be found. If the phase evolution of the nth carrier, $\phi_n(t)$, and mth carrier, $\phi_m(t)$ is known, the phase evolution of the remaining carriers can be written as:

$$\phi_k(t) = \phi_n(t) + \frac{k-n}{m-n}[\phi_m(t) - \phi_n(t)]. \tag{4}$$

This property is of importance when aiming at utilizing the spectral coherence between the carriers provided by a frequency comb. From this equation, one can easily realize that in the ideal case by transmitting two unmodulated lines, e.g., two pilot tones, a frequency comb with the same individual phases as the transmitter carriers can be generated at the receiver side and therefore perform self-homodyne detection. We will refer to this technique as comb-regeneration for self-homodyne superchannel detection. We will here discuss several techniques, illustrated in Figure 5, that have already been demonstrated to regenerate a frequency comb.

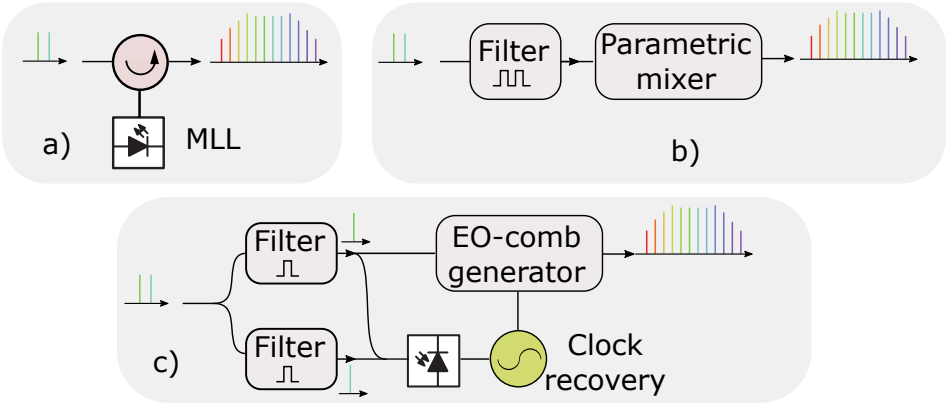

Figure 5. Schematic of different methods for regenerating a frequency comb using (**a**) a mode-locked laser (MLL), (**b**) a parametric mixer (cascaded four-wave mixing) and (**c**) an electro-optic (EO) comb with external clock recovery.

The first technique is injecting the two neighboring unmodulated lines and performing optical injection locking of a mode-locked laser, as shown in Figure 5a. This technique was already proposed in 2008 [89], although it was not shown that the quality of the regenerated frequency comb was sufficient to perform self-homodyne detection.

More recently, we demonstrated that by having two unmodulated lines and using four-wave mixing [63,64], a frequency comb can be all-optically regenerated. The main challenge of this technique is that the OSNR of the unmodulated lines must be sufficiently high to avoid undesired noise beating in the comb regeneration. Given that the pilot tones are co-transmitted with the data that are subject to the in-line amplifier noise, this can be a significant practical challenge. Therefore, optical filtering of these two unmodulated lines is of great importance. The first attempt to do this was based on optical injection-locked lasers [63], but achieving a filtering bandwidth below hundreds of MHz was still challenging with this technique. However, the filtering is critical to achieve successful comb regeneration. By exploiting the narrow bandwidth of Brillouin amplification, we demonstrated the first successful self-homodyne detection using a regenerated comb in [64]. While the Brillouin amplification

provided around 25 MHz of filtering, the noise added in this stage and the extinction ratio of the filtering (i.e., the gain of the amplifier) limited the number of regenerated carriers that could be used for self-homodyne detection to around 24 carriers.

Another possible technique is the use of an electrical phase-locked loop (PLL) for retrieving the frequency separation among the carriers [65]. In this case, two neighboring carriers are beat in a photodiode, and the frequency separation is obtained and filtered by a PLL. The output of the PLL was then used to drive an EO comb. While this technique was demonstrated for an EO comb, it could also be implemented in any comb that uses an RF driving signal. In addition, this technique could be implemented for combs that can be seeded by two lines such as parametric combs or Kerr combs. In such a case, the two lines seeding the comb could be realized by a simple EO modulation stage. However, this technique will be limited by the bandwidth of the PLL, and PLL power consumption might become an issue.

So far, we have mainly discussed techniques of adjacent pilot tones. Using non-adjacent tones is also viable, however at the expense of a more complex comb regeneration scheme. For example, in the case of the PLL, one could consider transmitting the central lines and an outer line. The regenerated comb would use the central line as the seeding wave. To obtain the frequency spacing, one could detect the phase variations between the other pilot tone and a carrier of the regenerated comb neighboring or at the same location as this pilot tone. The use of two unmodulated lines at each side of the comb has been used to improve the phase noise of the carriers generated by a gain-switched laser [90]. Similarly in the case of obtaining the frequency spacing from a data channel processed through DSP, this channel is not required to be at any specific location, although its location must be accounted for.

In the context of SDM, comb regeneration has been demonstrated by dedicating one core of a multi-core fiber to transmission of a set of comb pilots [91], whereas the data were transmitted in the remaining cores. The comb was detected in a photodiode in order to obtain the frequency spacing, and the obtained RF signal then drove a modulator seeded by the pilot comb. Frequency estimation was not included in the DSP, but carrier phase estimation was performed. We should note that this demonstration was performed with QPSK modulation only and that the comb regeneration was enabled by the high OSNR of the comb at the receiver side.

3.3. Regeneration from a Single Pilot

Apart from transmitting two lines as pilot signals, a single pilot can be used for regeneration as demonstrated in [92] and more recently [67]. However, the issue becomes the accuracy of the frequency spacing between the comb lines, which will be related to the stability of the electric clocks that generate the lines in the transmitter and receiver. We have measured that our 25-GHz RF clocks have frequency variations of about ± 15 kHz over several days, which can impact detection. These variations could be even larger when the two clocks are in different locations, since their temperature-dependent frequency-change is on the order of 0.1–1 kHz per degree change. In addition, the phase noise from the clock will impose a phase noise in each optical carrier whose variance increases with carrier number. While two extremely frequency stable combs would allow one to simplify the comb regeneration to just recovering a pilot tone, in most cases, the frequency spacing should also be tracked. As will be shown in Section 4, the phase noise of two independent RF clocks impairs performance, which increases with the number of transmitted carriers.

Another possibility could be using the digital information to tune the RF clock in DSP. The effectiveness of this technique will depend on how fast the frequency spacing varies and the latency of the data processing and accuracy. This technique would be an intermediate step between the techniques presented here for comb regeneration in a self-homodyne system and joint processing that will be presented in Section 4 and has to our knowledge never been demonstrated.

Provided the frequency stability of the regenerated lines is sufficient, the single-pilot scheme will lead to reduced DSP complexity by eliminating the need for frequency carrier recovery [67]. It also reduces phase noise and the risk of cycle slips. In addition, by performing carrier-phase estimation,

effects from fiber nonlinearities are mitigated [93,94]. Therefore, despite not reducing DSP complexity as much as dual-pilot comb regeneration, transmitting a single shared optical pilot tone is a technique of great interest, due to its lower overhead and reduced-complexity comb-regeneration. When combined with a digital pilot-symbol-based carrier recovery, single-pilot tone schemes can enable very low pilot overheads and record spectral efficiency [68].

A related technique is so-called seed-light wave distribution, where the pilot tone is not multiplexed with the signal, but instead, transmitted on a separate fiber. This concept was demonstrated by Sakaguchi et al. [95,96] by transmitting 10-GBaud PM-64QAM modulated on the lines of an EO-comb. The seed laser for the transmitter comb was transmitted on a separate fiber and used to seed the LO EO-comb, which enabled the signals to be received without a dedicated carrier-phase estimation stage in the DSP.

3.4. Effects of Dispersion and Noise

When implementing comb regeneration for self-homodyne applications, there are several aspects that need to be taken into consideration. The OSNR of the pilots tones seeding the receiver comb is one aspect, as in all-optical comb regeneration the OSNR of the lines seeding the receiver comb will determine the quality of the regenerated comb. Amplified-spontaneous-emission (ASE) noise on the carriers seeding the comb imposes a phase noise on the carriers and will therefore impact the regenerated comb. Due to scaling of the phase noise with line number, very narrow filtering of the seeding carriers is desired; however, care must be taken that the filtering is still larger than the clock variations. Assuming that the OSNR of the pilot tones is similar to that of the data channels, and not to impact the comb regeneration, we would like that $\mathrm{BW}_{\mathrm{filter}}/R_s \ll n^2$ [64] where $\mathrm{BW}_{\mathrm{filter}}$ is the filter bandwidth, R_s is the symbol rate and n is the number of carriers that are transmitted. For this reason, obtaining and filtering the line spacing in the electrical domain (e.g., using a PLL as discussed above) is desirable since narrow-bandwidth filters are available. We should note that in this case, the carrier seeding the receiver comb should also be filtered to avoid penalties, but a filter with much lower bandwidth than the symbol rate is sufficient.

Apart from the OSNR, the phase correlation among the unmodulated tones will be affected by, e.g., dispersion during the transmission. As has been studied [63], the quality of the regenerated comb can be affected by the dispersive walk-off. If we assume a link with electronic dispersion compensation, the dispersive walk-off between the carriers together with the phase-noise scaling in parametric optical frequency combs [97] can be used to find that the comb regeneration requires $n^2T \ll T_c$ [63] where T_c is the coherence time of the laser and T is the time delay between the two unmodulated carriers induced by dispersion walk off. This quantifies how dual-pilot comb regeneration for self-homodyne detection is sensitive to dispersive walk-off. This effect can be compensated by either using inline dispersion compensation or by just using a delay line to compensate for the walk-off among the pilots. Another effect to account for is the dispersive walk off between the data channels and the pilot tones. If we assume that the delay between pilot tones is compensated for, the phase difference between the regenerated local oscillators and the data channel suffering from highest walk off is given by nT. Therefore, in order not to be penalized, we require the walk-off to be much smaller than the laser coherence time, $nT \ll T_c$, which is a less stringent condition than the above.

4. Joint Digital Signal Processing Schemes for Carrier Recovery

In this section, we discuss how the phase coherence of the channels in a frequency comb-based system can be utilized by joint processing in the digital domain. In contrast to the methods described in Section 3, this section focuses on DSP-based algorithms and methods for systems with free-running LO-combs without pilot tones. It is partly based on the work presented in [66]. As previously discussed, the principles of joint processing are similar regardless of the physical principles of the phase locking. We therefore review the previous work on joint carrier recovery also for SDM systems.

The most basic system where joint carrier recovery is possible is in fact a standard dual-polarization signal, which was demonstrated early in the development of digital coherent receivers [98]. More recently, joint-polarization phase-noise estimation was studied for a pilot-base algorithm and shown to be able to both increase phase-noise tolerance and reduce the pilot rate [99]. In more advanced SDM systems, joint phase-tracking has been demonstrated in multicore [100] and multimode [101,102] fiber. Both of these demonstrations focused on reducing the DSP complexity.

For comb-based spectral superchannels, joint phase tracking was first proposed by Liu et al. [103]. Using simulations they showed that the phase noise tolerance increased when processing three channels together. However, before that, Souto et al. [104] demonstrated joint processing of two subchannels generated electrically and modulated on a single laser line. The subchannels were detected in a single coherent receiver and jointly processed to achieve a higher phase noise tolerance. In the system proposed in [82], an optical frequency comb was used to generate a spectral superchannel, which was detected in a single ultra-broadband coherent receiver using a single LO line. The subchannels were then jointly processed using a pilot-aided phase estimation algorithm. For comb-based superchannels with a comb as LO, we demonstrated joint carrier recovery in [66].

4.1. Algorithms for Joint Carrier Recovery

The carrier recovery stage of the DSP chain is typically divided into a coarse frequency offset estimation part and a fine carrier phase estimation part. The coarse frequency offset estimation can be performed relatively seldom since the frequency offset varies only slowly. In contrast, the fine phase estimation needs to be able to track rapid phase fluctuations originating from the phase noise of the transmitter and LO laser. This makes it more demanding, both in terms of computational complexity and performance. Therefore, most of the focus of joint carrier recovery schemes is on the fine phase tracking. Carrier recovery can be performed either in a blind fashion or aided by pilot symbols. Here, we focus on blind methods. Further discussion on pilot-aided joint phase noise estimation can be found in [105,106].

There are two main strategies to joint phase tracking, illustrated in Figure 6, that have different objectives and benefits. The first scheme is best described as master-slave phase tracking and aims to share the computational resources needed for phase estimation between the several channels that share the same phase-noise. As the name implies, the phase estimated from a master channel is applied to the other, slave channels. The second strategy can be described as a joint-estimation scheme, where the phase is estimated from all the channels, and the additional phase information is used to improve the phase estimation. The two strategies are described in more detail below.

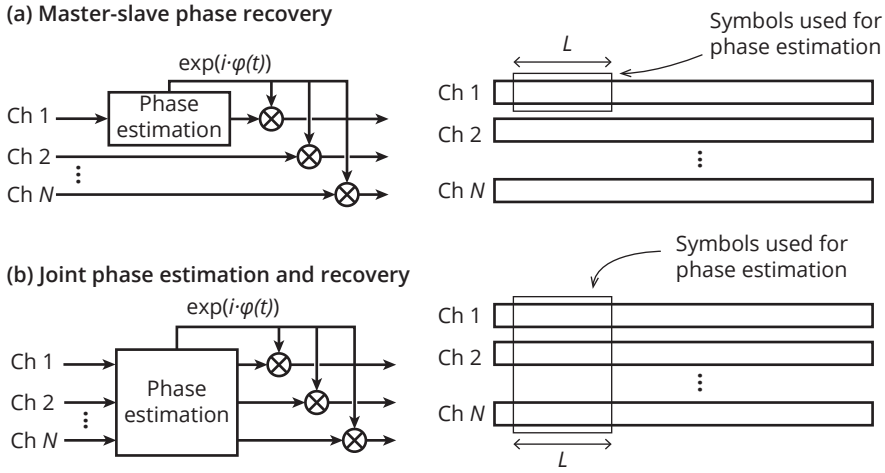

Figure 6. Principle of (**a**) master-slave phase recovery and (**b**) joint phase estimation.

4.1.1. Master-Slave Carrier Recovery

Master-slave carrier recovery is relatively straight forward. The frequency offset and phase is estimated from the master channel and then applied to the slave channels. The main principle does not depend on the algorithm used for the master frequency and phase estimation as long as the estimated frequency and phase can be readily extracted and applied to the slave channels.

There are different motivations for using master-slave schemes for phase estimation and frequency offset estimation. For phase estimation, the underlying rationale is that the phase estimation is computationally demanding and therefore attractive to share between many channels. Master-slave frequency offset estimation on the other hand can be used to avoid frequency offset differences between the channels. Traditional fourth-power spectral methods to estimate the frequency offset generally have a limited frequency resolution [107], which leads to a small frequency offset remaining on the signal. This offset is easily tracked with the fine phase estimator, but it might be different for different channels and therefore hinders joint phase recovery.

Master-slave frequency offset compensation however requires some additional considerations depending on the specific LO comb implementation. If the spacings of the transmitter and LO combs are synchronized, the channels will have the same frequency offset, and the master-slave concept can be directly used. However, if the spacings are not synchronized, the channels will have different frequency offsets. In this case, the comb spacing difference needs to be estimated separately and also applied to the slave channels. The principle of such a scheme is illustrated in Figure 7a. The comb spacing generally varies only slowly and can be estimated relatively seldomly.

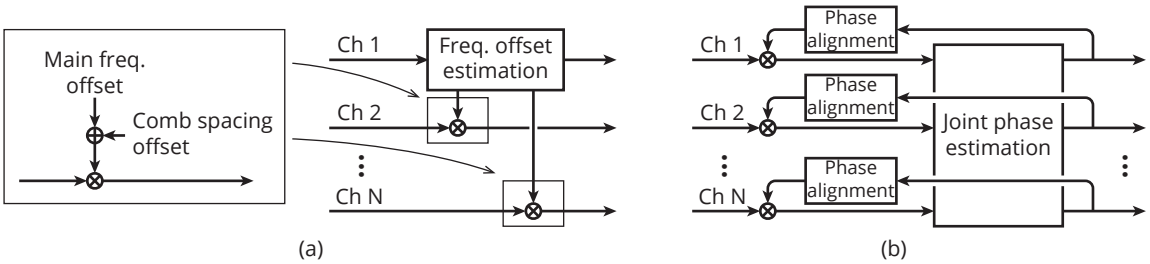

Figure 7. (**a**) Master-slave frequency offset compensation for unsynchronized combs; (**b**) feedback phase alignment for joint phase estimation.

4.1.2. Joint Phase Estimation

Traditional, single-channel phase estimation schemes typically apply time-averaging filters on the estimated phase to remove the effects of additive noise. Since longer time-averaging decreases the ability to track fast phase changes, this creates a tradeoff between noise sensitivity and phase-noise tracking speed. The benefit of multi-channel phase estimation is that the averaging block can be extended to include several channels, which improves the tolerance to additive noise without increasing the time averaging length, thus increasing phase noise tolerance. In short, the SNR of the phase estimation can be increased without negatively affecting the tracking speed.

Blind phase-search (BPS) [108] is a popular blind phase-estimation algorithm since it can be implemented in parallel without degrading tracking speed. Here, we describe how BPS can be extended to multiple channels. In the BPS algorithm, the received signal Z_k, sampled at symbol rate, is first rotated with B test phase angles:

$$\phi_b = \frac{b}{B} \cdot \frac{\pi}{2}, \tag{5}$$

where b is the index of the test angles. Then, the distance to the closest constellation symbol is calculated as:

$$|d_{k,b}|^2 = |Z_k e^{-j\phi_b} - [Z_k e^{-j\phi_b}]_D|^2, \tag{6}$$

where $[\cdot]_D$ denotes symbol decision. In a traditional BPS algorithm, the distances are then averaged over $L+1$ consecutive symbols to reduce the impact of additive noise. When extending the algorithm to multiple channels, the averaging is extended to C channels, as well. This is described by:

$$e_{k,b} = \sum_{c=1}^{C} \sum_{\ell=-L/2}^{L/2} |d_{c,k-\ell,b}|^2, \tag{7}$$

where we added a channel index c to the distance. The estimated phase angle is chosen as the one that minimizes $e_{k,b}$. The length of the summing window $L+1$ is what determines the phase-tracking speed, where a smaller L gives a higher tracking speed. The total number of symbols used for the estimation, which determines the tolerance to additive noise, is $N = C \cdot (L+1)$. In multichannel cases, the summing window length can be reduced by a factor of C, which leads to a higher phase-noise tolerance, while maintaining the same tolerance to additive noise.

4.1.3. Managing Channel Phase Differences

Channel phase differences mainly arise from the comb generation process, but can also be caused by vibrations and temperature-induced changes when the different channels travel through different fibers. Since the joint carrier recovery schemes rely on the phases being the same, performance may be affected.

In the case of master-slave carrier recovery, any phase difference will remain on the slave channels after the master phase has been applied to them. Performance-wise, it is no major challenge to remove these since they are typically much smaller than the common-mode phase noise. However, since the goal of the master-slave type of scheme is to reduce the DSP computational complexity, it is important that the phase difference compensation is computationally lightweight compared to the master phase estimator. For small phase differences, an adaptive equalizer will be able to perform the compensation provided that the error signal used for the tap update is sensitive to phase rotations. In this case, the main adaptive equalizer that performs polarization demultiplexing will also track phase differences. Another alternative is to use a separate feedback phase tracker, since they are computationally lightweight if the tracking-speed requirements are low.

The joint-estimation schemes have different requirements. To not affect the main phase estimation, the phases of the channels need to be aligned before the joint estimation block. For example, in the modified BPS algorithm described above, a large phase difference between the channels will cause the cost function in Equation (7) to have multiple local minima, corresponding to the different channels. This will cause rapidly-varying estimation errors that are hard to compensate at a later stage in the DSP chain.

The challenge of aligning the phases before the joint phase estimation block is that the channel-dependent phase noise is much smaller than the common phase noise among the lines and cannot be estimated easily before the common phase noise has been compensated for. This can be solved by using a feedback method where the remaining phase error after joint phase compensation is used to align the channels before the joint estimation. This is illustrated in Figure 7b. In a practical hardware implementation, the updating speed of such a phase-tracker will be limited by parallelization [108] and ultimately limit the allowable speed of the channel-dependent phase noise.

4.2. Transmission Effects

Fiber transmission will affect the phase coherence between the channels in mainly two ways. First, dispersive walk-off will cause a delay between the channels, which will affect the performance

of the joint processing. Here, it is important to realize that this cannot be compensated for by simply applying electronic delays to the detected channels since the the phase noise originates from both the carrier and the LO laser. If the channels are time-shifted relative to each other before detection, they will mix with different parts of the LO phase noise. Thus, the phase noise differences cannot be undone by simply time-shifting the detected signals. Second, fiber nonlinearities may introduce phase noise on the channels. However, the effects of this on joint processing remains to be studied.

4.3. Experimental Evaluation

In [66], we experimentally investigated master-slave carrier recovery in comb-based receivers. Using the same setup, we also investigated joint phase estimation. In the setup, two free-running EO frequency combs with 25-GHz spacing were used as transmitter and LO light sources, and two 10-GBaud PM-64QAM subchannels were transmitted and received at the same time. This enabled us to perform proof-of-concept demonstrations for a back-to-back case.

First, we studied the phase correlation between the channels. This was done by performing separate phase tracking on the two simultaneously-received channels and comparing the resulting phase traces. In Figure 8, the phase traces for two frequency spacings, 25 GHz and 275 GHz, are plotted together with their difference. In both cases, the phases are similar enough to be nearly indistinguishable when plotted on top of each other. However, when the phase difference is plotted separately, a small, but noticeable difference can be seen for the 275-GHz spacing case. Indeed, as seen in Figure 8c, the standard deviation of the phase difference increases with the frequency spacing. With the addition of some measurement noise, the increase is approximately linear with frequency spacing, in agreement with Equation (1).

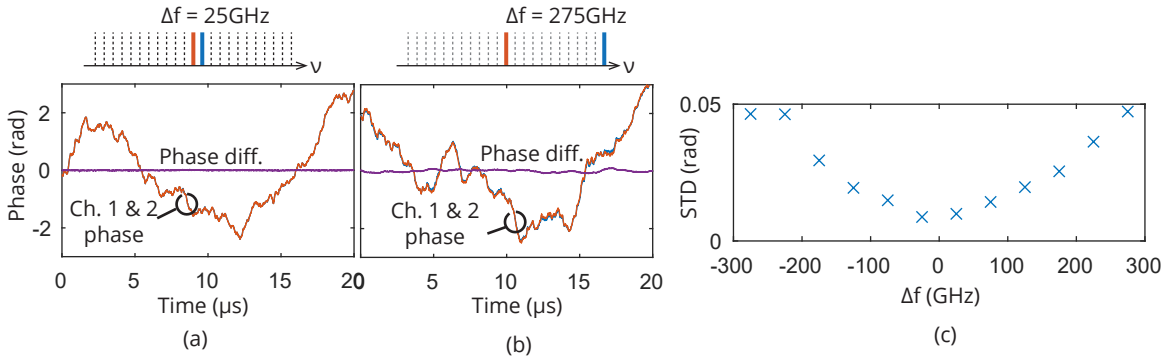

Figure 8. (**a**) Phase traces from channels spaced $\Delta f = 25$ GHz apart, together with their difference; (**b**) phase traces from channels spaced $\Delta f = 275$ GHz apart, together with their difference; (**c**) phase difference standard deviation (STD) as a function of channel frequency spacing.

4.3.1. Master-Slave

The joint carrier recovery was implemented by doing coarse frequency offset estimation and phase estimation on the master channel. The estimated frequency offset and phase noise was then applied to the slave channel. Since the combs were unsynchronized, they had a small spacing difference of ∼30 kHz. This difference was measured once and used as a correction factor when the master frequency offset was applied to the slave channels, as illustrated in Figure 7a. After applying the master phase to the slave channels, a slow feedback-based phase tracker was used to compensate the small phase variations remaining.

4.3.2. Joint Estimation

We evaluated joint phase estimation with the same setup as in [66], but with a distributed feedback (DFB) laser as the seed for the transmitter. The DFB laser had a specified linewidth of 1 MHz and

was chosen to evaluate the phase noise tolerance of the joint phase estimation. The algorithm used was the modified BPS described in Section 4.1.2. Frequency offset compensation was performed in a master-slave fashion as illustrated in Figure 7a. To align the phase before joint estimation, a feedback-based phase-aligner as described in Figure 7b was applied. The phase alignment was implemented as a one-tap decision-directed equalizer, where the tap was updated every 128th symbol.

The phase-estimation algorithms were evaluated for channel separations of up to ±275 GHz. We compared independent phase estimation, joint-polarization and joint-wavelength phase estimation, which means that the phase estimation is performed on 1, 2 and 4 polarization channels, respectively. To make a fair comparison, the feedback-based phase alignment was applied in all cases.

In Figure 9a,b, the bit-error rate (BER) for the center channel is plotted as a function of averaging filter time window for the three cases, with frequency spacing of 125 GHz and 275 GHz away. This corresponds to five and 11 wavelength channels away, respectively. For the same averaging time window, the joint schemes used two- or four-times more symbols for averaging due to having access to more channels. Both the joint-polarization and joint-wavelength phase-estimation schemes consistently performed better than the single-polarization phase estimation in terms of BER and had a shorter optimum averaging time window, which is expected. The catastrophic failures for short block lengths seen in Figure 9a,b were caused by cycle slip events, and an increased number of jointly-processed channels improve the resilience against these events. In terms of BER, the joint-wavelength scheme performed better than the joint-polarization scheme with 125-GHz frequency spacing, but for a spacing of 275 GHz, which was the furthest tested, the BER performance of the two joint schemes is similar. The higher resilience against cycle slips was however retained also for the higher spacing.

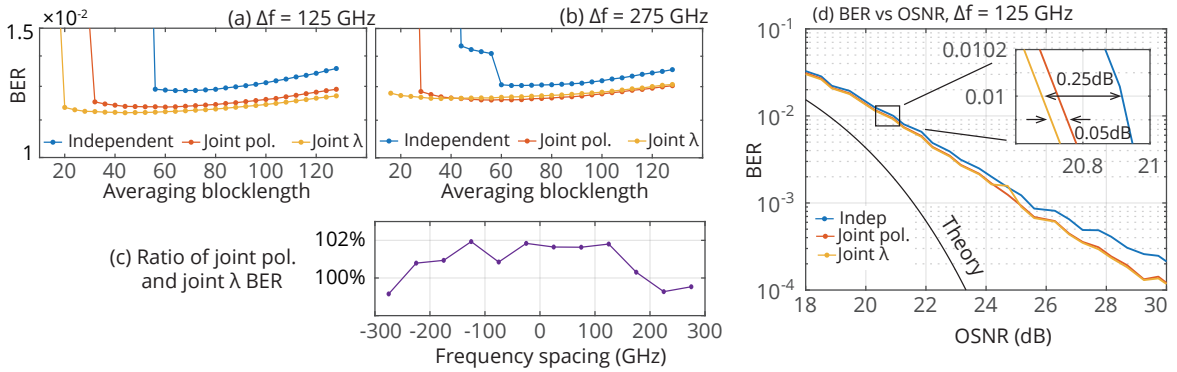

Figure 9. (**a**,**b**) Bit-error rate (BER) of the center channel as a function of the filter block-length, with either independent, joint-polarization or joint-wavelength phase estimation for different frequency spacings to the other wavelength channel. The optical signal-to-noise ratio (OSNR) is 20.3 dB. (**c**) The ratio between the BER for joint-polarization and joint-wavelength phase estimation as a function of frequency spacing. The optimal block length is used in all cases. OSNR ≅ 20 dB. (**d**) BER vs. OSNR for a frequency spacing of 125 GHz. The block lengths are 96, 48 and 32 for independent, joint polarization and joint wavelength, respectively, which are close to the optimum values. The theoretical curve corresponds to an additive white Gaussian-noise channel assuming Gray-coding and only nearest neighbor errors [109].

In Figure 9c, the ratio between the BER achieved by the joint-polarization and the joint-wavelength schemes is plotted as a function of the frequency spacing. Up to a frequency spacing of 175 GHz, the joint-wavelength scheme performed better than the joint-polarization, but for larger frequency spacings, this gain is diminished. This was likely due to the frequency-spacing-dependent phase-noise differences between the comb lines observed in [66]. In Figure 9d, the BER is plotted as a function of the OSNR for a frequency spacing of 125 GHz. We observe a 0.25-dB lower required OSNR for

BER $= 10^{-2}$ for the joint-wavelength case compared to the independent case. The difference between the joint schemes is only 0.05 dB.

Although the performance gains were small, they are consistent for the tested frequency spacings and OSNR values. This indicates that the results were not a statistical artifact. The fact that the performance gain is small means that phase noise was not a limiting factor in the tested system. Instead, our results serve as an indication that the phase coherence between the received channels was good enough to enable joint phase estimation. In phase-noise limited systems, such as low-baud rate and higher-order modulation-format systems, larger performance gains can be expected, which has been demonstrated in other phase-locked systems [104] and predicted using simulations [99,103,105].

Although we have discussed master-slave methods and joint phase estimation separately, these two methods can be readily combined if several subchannels are present. The design strategy could then be to perform joint phase estimation on a subset of the channels, enough to reach the desired phase noise tolerance, and then use the jointly estimated phase for the remaining subchannels in a master-slave fashion. Then, both increased phase-noise tolerance and complexity reduction can be achieved.

5. Conclusions and Outlook

In this paper, we have reviewed optical frequency combs and their use as light sources for spectral superchannels. We have described several methods for utilizing the phase coherence of the subchannels provided by frequency combs, both analog methods for comb regeneration and digital joint-DSP methods. In addition, we have discussed practical challenges when implementing comb-based superchannels, both general and specific to experiments. The work summarized in this paper shows the potential for both performance improvements and power consumption savings made possible by joint processing in comb-based fiber-optical systems. In addition, the phase-locked carriers from an optical frequency comb also reduce the need for guard bands between subchannels and thus enables an increased spectral efficiency compared to using free-running lasers.

Applications where these approaches could be advantageous include short-reach links with higher order modulation formats where the transmission distance is limited, since in this case, the phase estimation part of the DSP plays a bigger role in the power consumption. Joint processing also has the potential to lessen the linewidth requirements on integrated comb sources, which might pave the way for their usage in compact superchannel transceivers.

5.1. Comparison of the Methods in This Paper

Both analog and digital methods have specific benefits and challenges. Analog methods for comb regeneration inevitably add hardware complexity, but the digital parts of the receivers can be operated independently. Digital methods require all subchannels to be processed in the same DSP application-specific integrated circuit (ASIC) or have ASICs synchronized, which could be challenging for a large number of subchannels. On the other hand, for analog methods, the added complexity for joint processing does not scale with the number of subchannels. Therefore, analog methods are more suitable for massive superchannels with a large number of subchannels, while digital methods are more suitable for smaller superchannels. This is further accentuated by the fact that analog methods require pilot tones, which often reduces the spectral efficiency.

Nevertheless, there are scenarios where digital methods can be implemented essentially for free. This is the case in superchannel systems that already rely on some joint DSP, such as multiple-input multiple-output (MIMO) equalization for crosstalk mitigation [103]. Then, the subchannel receivers already need to be synchronized, and joint carrier recovery can be readily implemented.

5.2. Future Outlook

There are several prospective future research areas related to joint processing in comb-based systems. The first one deals with the limitations of joint processing in terms of transmission

distance. So far, the transmission experiments have been limited to single spans or back-to-back. Fiber transmission comes with the additional challenges of dispersion that will cause a walk-off between the subchannels, as well as fiber nonlinearities that will cause additional phase noise. To fully understand how these effects affect joint processing, long-haul transmission experiments need to be performed.

A second interesting area is the possibility for co-integration of comb-sources and transceivers. The demonstrations of joint processing described in this work were based on discrete-component EO-combs. While EO-combs can be integrated on a single chip [110], other promising comb-sources are microring resonators [52] and quantum-dash mode-locked lasers [36]. Furthermore, quantum-dot mode-locked lasers show high phase coherence [111,112]. For these comb-sources, joint processing remains to be demonstrated.

The third area is understanding the full implementation aspects of joint processing. The benefits of frequency combs as light sources combined with joint processing depend on the cost and power consumption of several parts of the transceiver. Thus, a wide tradeoff analysis including the power consumption of lasers, comb generation and DSP ASICs is needed.

Fourth, the potential for combining SDM, frequency combs and joint processing should be further investigated. Utilizing frequency combs in SDM transmission has been demonstrated [28], as well as joint processing in SDM systems [100,101]. In [91], the receiver comb was regenerated using a set of pilot tones transmitted in a separate core. Combining pilot tones and data channels in the same core would lower the overhead further. In addition, also joint-DSP methods could potentially be extended to utilize both spectral and spatial phase coherence.

Author Contributions: M.K. and V.T.-C. planned and wrote Section 1. M.M. and M.K. planned and wrote Section 2. A.L.-R. and M.K. planned and wrote Section 3. L.L. planned and wrote Sections 4 and 5. The experiments reported in Section 4 were planned and performed by L.L. with support from M.M. and A.L.-R. L.L. took the overall responsibility in managing the manuscript. M.K., J.S. and P.A.A. supervised the work and provided technical leadership. All co-authors contributed to the final version with suggestions and critical comments.

Acknowledgments: This work was financially supported by the Swedish research council and the Knut and Alice Wallenberg foundation.

Conflicts of Interest: The authors declare no conflict of interest.

References

1. Mears, R.; Reekie, L.; Jauncey, I.; Payne, D. Low-noise erbium-doped fibre amplifier operating at 1.54 μm. *Electron. Lett.* **1987**, *23*, 1026–1028. [CrossRef]
2. Desurvire, E.; Simpson, J.R.; Becker, P.C. High-gain erbium-doped traveling-wave fiber amplifier. *Opt. Lett.* **1987**, *12*, 888–890. [CrossRef] [PubMed]
3. Fishman, D.A.; Nagel, J.A.; Cline, T.W.; Tench, R.E.; Pleiss, T.C.; Miller, T.; Coult, D.G.; Milbrodt, M.A.; Yeates, P.D.; Chraplyvy, A.; et al. A high capacity noncoherent FSK light wave field experiment using Er^{3+}-doped fiber optical amplifiers. *IEEE Photon. Technol. Lett.* **1990**, *2*, 662–664. [CrossRef]
4. Taga, H.; Yoshida, Y.; Edagawa, N.; Yamamoto, S.; Wakabayashi, H. 459 km, 2.4 Gbit/s four wavelength multiplexing optical fibre transmission experiment using six Er-doped fibre amplifiers. *Electron. Lett.* **1990**, *26*, 500–501. [CrossRef]
5. Bergano, N.S. Wavelength division multiplexing in long-haul transoceanic transmission systems. *J. Lightw. Technol.* **2005**, *23*, 4125–4139. [CrossRef]
6. Cai, J.X.; Batshon, H.G.; Mazurczyk, M.; Sinkin, O.V.; Wang, D.; Paskov, M.; Patterson, W.; Davidson, C.; Corbett, P.; Wolter, G.; et al. 70.46 Tb/s over 7600 km and 71.65 Tb/s over 6970 km Transmission in C+ L Band Using Coded Modulation with Hybrid Constellation Shaping and Nonlinearity Compensation. *J. Lightw. Technol.* **2017**, *36*, 114–121. [CrossRef]
7. Derr, F. Coherent optical QPSK intradyne system: Concept and digital receiver realization. *J. Lightw. Technol.* **1992**, *10*, 1290–1296. [CrossRef]
8. Sun, H.; Wu, K.; Roberts, K. Real-time measurements of a 40 Gb/s coherent system. *Opt. Exp.* **2008**, *16*, 873–879. [CrossRef]

9. Kobayashi, T.; Sueta, T.; Cho, Y.; Matsuo, Y. High-repetition-rate optical pulse generator using a Fabry-Perot electro-optic modulator. *Appl. Phys. Lett.* **1972**, *21*, 341–343. [CrossRef]
10. Kobayashi, T.; Yao, H.; Amano, K.; Fukushima, Y.; Morimoto, A.; Sueta, T. Optical pulse compression using high-frequency electrooptic phase modulation. *IEEE J. Quantum Electron.* **1988**, *24*, 382–387. [CrossRef]
11. Metcalf, A.J.; Torres-Company, V.; Leaird, D.E.; Weiner, A.M. High-Power Broadly Tunable Electrooptic Frequency Comb Generator. *IEEE J. Sel. Top. Quantum Electron.* **2013**, *19*, 231–236. [CrossRef]
12. Wu, R.; Supradeepa, V.R.; Long, C.M.; Leaird, D.E.; Weiner, A.M. Generation of very flat optical frequency combs from continuous-wave lasers using cascaded intensity and phase modulators driven by tailored radio frequency waveforms. *Opt. Lett.* **2010**, *35*, 3234. [CrossRef] [PubMed]
13. Weiner, A.; Metcalf, A.; Diddams, S.; Fortier, T.; Quinlan, F. Broadly tunable, low timing jitter, high repetition rate optoelectronic comb generator. *Electron. Lett.* **2015**, *51*, 1596–1598.
14. Keller, U. Recent developments in compact ultrafast lasers. *Nature* **2003**, *424*, 831–838. [CrossRef] [PubMed]
15. Ranka, J.K.; Windeler, R.S.; Stentz, A.J. Visible continuum generation in air–silica microstructure optical fibers with anomalous dispersion at 800 nm. *Opt. Lett.* **2000**, *25*, 25. [CrossRef] [PubMed]
16. Jones, D.J.; Diddams, S.A.; Ranka, J.K.; Stentz, A.; Windeler, R.S.; Hall, J.L.; Cundiff, S.T. Carrier-Envelope Phase Control of Femtosecond Mode-Locked Lasers and Direct Optical Frequency Synthesis. *Science* **2000**, *288*, 635–639. [CrossRef] [PubMed]
17. Holzwarth, R.; Udem, T.; Hänsch, T.W.; Knight, J.C.; Wadsworth, W.J.; Russell, P.S.J. Optical Frequency Synthesizer for Precision Spectroscopy. *Phys. Rev. Lett.* **2000**, *85*, 2264–2267. [CrossRef] [PubMed]
18. Morioka, T.; Takara, H.; Kawanishi, S.; Kamatani, O.; Takiguchi, K.; Uchiyama, K.; Saruwatari, M.; Takahashi, H.; Yamada, M.; Kanamori, T.; et al. 1 Tbit/s (100 Gbit/s times 10 channel) OTDM/WDM transmission using a single supercontinuum WDM source. *Electron. Lett.* **1996**, *32*, 906–907. [CrossRef]
19. Veselka, J.; Korotky, S. A multiwavelength source having precise channel spacing for WDM systems. *IEEE Photon. Technol. Lett.* **1998**, *10*, 958–960. [CrossRef]
20. Ohara, T.; Takara, H.; Yamamoto, T.; Masuda, H.; Morioka, T.; Abe, M.; Takahashi, H. Over-1000-channel ultradense WDM transmission with supercontinuum multicarrier source. *J. Lightw. Technol.* **2006**, *24*, 2311–2317. [CrossRef]
21. Ishizawa, A.; Nishikawa, T.; Mizutori, A.; Takara, H.; Aozasa, S.; Mori, A.; Nakano, H.; Takada, A.; Koga, M. Octave-spanning frequency comb generated by 250 fs pulse train emitted from 25 GHz externally phase-modulated laser diode for carrier-envelope-offset-locking. *Electron. Lett.* **2010**, *46*, 1343–1344. [CrossRef]
22. Jiang, Z.; Huang, C.B.; Leaird, D.E.; Weiner, A.M. Optical arbitrary waveform processing of more than 100 spectral comb lines. *Nat. Photon.* **2007**, *1*, 463–467. [CrossRef]
23. Ataie, V.; Temprana, E.; Liu, L.; Myslivets, E.; Kuo, B.P.P.; Alic, N.; Radic, S. Ultrahigh Count Coherent WDM Channels Transmission Using Optical Parametric Comb-Based Frequency Synthesizer. *J. Lightw. Technol.* **2015**, *33*, 694–699. [CrossRef]
24. Kuo, B.P.; Myslivets, E.; Ataie, V.; Temprana, E.G.; Alic, N.; Radic, S. Wideband Parametric Frequency Comb as Coherent Optical Carrier. *J. Lightw. Technol.* **2013**, *31*, 3414–3419. [CrossRef]
25. Wu, R.; Torres-Company, V.; Leaird, D.E.; Weiner, A.M. Supercontinuum-based 10-GHz flat-topped optical frequency comb generation. *Opt. Exp.* **2013**, *21*, 6045–6052. [CrossRef] [PubMed]
26. Temprana, E.; Ataie, V.; Kuo, B.P.P.; Myslivets, E.; Alic, N.; Radic, S. Low-noise parametric frequency comb for continuous C-plus-L-band 16-QAM channels generation. *Opt. Exp.* **2014**, *22*, 6822–6828. [CrossRef] [PubMed]
27. Gnauck, A.H.; Kuo, B.P.P.; Myslivets, E.; Jopson, R.M.; Dinu, M.; Simsarian, J.E.; Winzer, P.J.; Radic, S. Comb-Based 16-QAM Transmitter Spanning the C and L Bands. *IEEE Photon. Technol. Lett.* **2014**, *26*, 821–824. [CrossRef]
28. Puttnam, B.J.; Luis, R.S.; Klaus, W.; Sakaguchi, J.; Delgado Mendinueta, J.M.; Awaji, Y.; Wada, N.; Tamura, Y.; Hayashi, T.; Hirano, M.; et al. 2.15 Pb/s transmission using a 22 core homogeneous single-mode multi-core fiber and wideband optical comb. In Proceedings of the European Conference on Optical Communication (ECOC), Valencia, Spain, 27 September–1 October 2015, p. PDP.3.1.
29. Wang, Z.; Van Gasse, K.; Moskalenko, V.; Latkowski, S.; Bente, E.; Kuyken, B.; Roelkens, G. A III-V-on-Si ultra-dense comb laser. *Light Sci. Appl.* **2017**, *6*, e16260. [CrossRef]

30. Rafailov, E.U.; Cataluna, M.A.; Sibbett, W. Mode-locked quantum-dot lasers. *Nat. Photon.* **2007**, *1*, 395–401. [CrossRef]
31. Lu, Z.; Liu, J.; Poole, P.; Song, C.; Chang, S. Ultra-narrow linewidth quantum dot coherent comb lasers. In Proceedings of the Optical Fiber Communication Conference (OFC), San Diego, CA, USA 11–15 March 2018; p. Th1I.5.
32. Srinivasan, S.; Davenport, M.; Heck, M.J.R.; Hutchinson, J.; Norberg, E.; Fish, G.; Bowers, J. Low phase noise hybrid silicon mode-locked lasers. *Front. Optoelectron.* **2014**, *7*, 265–276. [CrossRef]
33. Roelkens, G.; Abassi, A.; Cardile, P.; Dave, U.; de Groote, A.; de Koninck, Y.; Dhoore, S.; Fu, X.; Gassenq, A.; Hattasan, N.; et al. III-V-on-Silicon Photonic Devices for Optical Communication and Sensing. *Photonics* **2015**, *2*, 969–1004. [CrossRef]
34. Vujicic, V.; Calo, C.; Watts, R.; Lelarge, F.; Browning, C.; Merghem, K.; Martinez, A.; Ramdane, A.; Barry, L.P. Quantum Dash Mode-Locked Lasers for Data Centre Applications. *IEEE J. Sel. Top. Quantum Electron.* **2015**, *21*, 53–60. [CrossRef]
35. Marin, P.; Pfeifle, J.; Kemal, J.N.; Wolf, S.; Vijayan, K.; Chimot, N.; Martinez, A.; Ramdane, A.; Lelarge, F.; Freude, W.; et al. 8.32 Tbit/s coherent transmission using a quantum-dash mode-locked laser diode. In Proceedings of the Conference on Lasers and Electro-Optics (CLEO), San Jose, CA, USA, 5–10 June 2016; p. STh1F.1.
36. Kemal, J.N.; Marin-Palomo, P.; Merghem, K.; Aubin, G.; Calo, C.; Brenot, R.; Lelarge, F.; Ramdane, A.; Randel, S.; Freude, W.; et al. 32QAM WDM transmission using a quantum-dash passively mode-locked laser with resonant feedback. In Proceedings of the Optical Fiber Communication Conference (OFC), Los Angeles, CA, USA, 19–23 March 2017; p. Th5C.3.
37. Zhou, R.; Huynh, T.N.; Vujicic, V.; Anandarajah, P.M.; Barry, L.P. Phase noise analysis of injected gain switched comb source for coherent communications. *Opt. Exp.* **2014**, *22*, 8120. [CrossRef] [PubMed]
38. Gutierrez Pascual, M.D.; Vujicic, V.; Braddell, J.; Smyth, F.; Anandarajah, P.M.; Barry, L.P. InP photonic integrated externally injected gain switched optical frequency comb. *Opt. Lett.* **2017**, *42*, 555. [CrossRef] [PubMed]
39. Kippenberg, T.J.; Holzwarth, R.; Diddams, S.A. Microresonator-Based Optical Frequency Combs. *Science* **2011**, *332*, 555–559. [CrossRef] [PubMed]
40. Del'Haye, P.; Schliesser, A.; Arcizet, O.; Wilken, T.; Holzwarth, R.; Kippenberg, T.J. Optical frequency comb generation from a monolithic microresonator. *Nature* **2007**, *450*, 1214–1217. [CrossRef] [PubMed]
41. Levy, J.S.; Gondarenko, A.; Foster, M.A.; Turner-Foster, A.C.; Gaeta, A.L.; Lipson, M. CMOS-compatible multiple-wavelength oscillator for on-chip optical interconnects. *Nat. Photon.* **2010**, *4*, 37–40. [CrossRef]
42. Huang, S.W.; Zhou, H.; Yang, J.; McMillan, J.F.; Matsko, A.; Yu, M.; Kwong, D.L.; Maleki, L.; Wong, C.W. Mode-Locked Ultrashort Pulse Generation from On-Chip Normal Dispersion Microresonators. *Phys. Rev. Lett.* **2015**, *114*, 053901. [CrossRef] [PubMed]
43. Pfeiffer, M.H.P.; Kordts, A.; Brasch, V.; Zervas, M.; Geiselmann, M.; Jost, J.D.; Kippenberg, T.J. Photonic Damascene process for integrated high-Q microresonator based nonlinear photonics. *Optica* **2016**, *3*, 20–25. [CrossRef]
44. Xuan, Y.; Liu, Y.; Varghese, L.T.; Metcalf, A.J.; Xue, X.; Wang, P.H.; Han, K.; Jaramillo-Villegas, J.A.; Al Noman, A.; Wang, C.; et al. High-Q silicon nitride microresonators exhibiting low-power frequency comb initiation. *Optica* **2016**, *3*, 1171–1180. [CrossRef]
45. Ji, X.; Barbosa, F.A.S.; Roberts, S.P.; Dutt, A.; Cardenas, J.; Okawachi, Y.; Bryant, A.; Gaeta, A.L.; Lipson, M. Ultra-low-loss on-chip resonators with sub-milliwatt parametric oscillation threshold. *Optica* **2017**, *4*, 619–624. [CrossRef]
46. Li, Q.; Briles, T.C.; Westly, D.A.; Drake, T.E.; Stone, J.R.; Ilic, B.R.; Diddams, S.A.; Papp, S.B.; Srinivasan, K. Stably accessing octave-spanning microresonator frequency combs in the soliton regime. *Optica* **2017**, *4*, 193–203. [CrossRef] [PubMed]
47. Levy, J.S.; Saha, K.; Okawachi, Y.; Foster, M.A.; Gaeta, A.L.; Lipson, M. High-Performance Silicon-Nitride-Based Multiple-Wavelength Source. *IEEE Photon. Technol. Lett.* **2012**, *24*, 1375–1377. [CrossRef]
48. Pfeifle, J.; Brasch, V.; Lauermann, M.; Yu, Y.; Wegner, D.; Herr, T.; Hartinger, K.; Schindler, P.; Li, J.; Hillerkuss, D.; et al. Coherent terabit communications with microresonator Kerr frequency combs. *Nat. Photon.* **2014**, *8*, 375–380. [CrossRef] [PubMed]

49. Wang, P.H.; Ferdous, F.; Miao, H.; Wang, J.; Leaird, D.E.; Srinivasan, K.; Chen, L.; Aksyuk, V.; Weiner, A.M. Observation of correlation between route to formation, coherence, noise, and communication performance of Kerr combs. *Opt. Exp.* **2012**, *20*, 29284–29295. [CrossRef] [PubMed]
50. Fülöp, A.; Mazur, M.; Lorences-Riesgo, A.; Eriksson, T.A.; Wang, P.H.; Xuan, Y.; Leaird, D.E.; Qi, M.; Andrekson, P.A.; Weiner, A.M.; et al. Long-haul coherent communications using microresonator-based frequency combs. *Opt. Exp.* **2017**, *25*, 26678–26688. [CrossRef] [PubMed]
51. Herr, T.; Brasch, V.; Jost, J.D.; Wang, C.Y.; Kondratiev, N.M.; Gorodetsky, M.L.; Kippenberg, T.J. Temporal solitons in optical microresonators. *Nat. Photon.* **2014**, *8*, 145–152. [CrossRef]
52. Marin-Palomo, P.; Kemal, J.N.; Karpov, M.; Kordts, A.; Pfeifle, J.; Pfeiffer, M.H.P.; Trocha, P.; Wolf, S.; Brasch, V.; Anderson, M.H.; et al. Microresonator-based solitons for massively parallel coherent optical communications. *Nature* **2017**, *546*, 274–279. [CrossRef] [PubMed]
53. Liao, P.; Bao, C.; Kordts, A.; Karpov, M.; Pfeiffer, M.H.P.; Zhang, L.; Cao, Y.; Almaiman, A.; Mohajerin-Ariaei, A.; Tur, M.; et al. Pump-linewidth-tolerant wavelength multicasting using soliton Kerr frequency combs. *Opt. Lett.* **2017**, *42*, 3177–3180. [CrossRef] [PubMed]
54. Bao, C.; Zhang, L.; Matsko, A.; Yan, Y.; Zhao, Z.; Xie, G.; Agarwal, A.M.; Kimerling, L.C.; Michel, J.; Maleki, L.; et al. Nonlinear conversion efficiency in Kerr frequency comb generation. *Opt. Lett.* **2014**, *39*, 6126–6129. [CrossRef] [PubMed]
55. Xue, X.; Xuan, Y.; Liu, Y.; Wang, P.H.; Chen, S.; Wang, J.; Leaird, D.E.; Qi, M.; Weiner, A.M. Mode-locked dark pulse Kerr combs in normal-dispersion microresonators. *Nat. Photon.* **2015**, *9*, 594–600. [CrossRef]
56. Xue, X.; Wang, P.H.; Xuan, Y.; Qi, M.; Weiner, A.M. Microresonator Kerr frequency combs with high conversion efficiency. *Laser Phot. Rev.* **2017**, *11*, 1600276. [CrossRef]
57. Fülöp, A.; Mazur, M.; Lorences-Riesgo, A.; Wang, P.H.; Xuan, Y.; Leaird, D.E.; Qi, M.; Andrekson, P.A.; Weiner, A.M.; Torres-Company, V. High-order coherent communications using mode-locked dark-pulse Kerr combs from microresonators. *Nature Communications* **2018**, *8*, 1598. [CrossRef] [PubMed]
58. Matsko, A.B.; Maleki, L. On timing jitter of mode-locked Kerr frequency combs. *Opt. Exp.* **2013**, *21*, 28862–28876. [CrossRef] [PubMed]
59. Liang, W.; Eliyahu, D.; Ilchenko, V.S.; Savchenkov, A.A.; Matsko, A.B.; Seidel, D.; Maleki, L. High spectral purity Kerr frequency comb radio frequency photonic oscillator. *Nat. Commun.* **2015**, *6*, 7957. [CrossRef] [PubMed]
60. Yi, X.; Yang, Q.F.; Zhang, X.; Yang, K.Y.; Li, X.; Vahala, K. Single-mode dispersive waves and soliton microcomb dynamics. *Nat. Commun.* **2017**, *8*, 14869. [CrossRef] [PubMed]
61. Takushima, Y.; Sotobayashi, H.; Grein, M.E.; Ippen, E.P.; Haus, H.A. Linewidth of mode combs of passively and actively mode-locked semiconductor laser diodes. Opt. East **2004**, *5595*, 213–227.
62. Newbury, N.R. Searching for applications with a fine-tooth comb. *Nat. Photon.* **2011**, *5*, 186–188. [CrossRef]
63. Lorences-Riesgo, A.; Eriksson, T.A.; Fülöp, A.; Andrekson, P.A.; Karlsson, M. Frequency-comb regeneration for self-homodyne superchannels. *J. Lightw. Technol.* **2016**, *34*, 1800–1806. [CrossRef]
64. Lorences-Riesgo, A.; Mazur, M.; Eriksson, T.A.; Andrekson, P.A.; Karlsson, M. Self-homodyne 24×32-QAM superchannel receiver enabled by all-optical comb regeneration using Brillouin amplification. *Opt. Exp.* **2016**, *24*, 29714–29723. [CrossRef] [PubMed]
65. Mazur, M.; Lorences-Riesgo, A.; Schroeder, J.; Andrekson, P.A.; Karlsson, M. 10 Tb/s PM-64QAM Self-Homodyne Comb-Based Superchannel Transmission with 4% Shared Pilot Tone Overhead. *J. Lightw. Technol.* **2018**. [CrossRef]
66. Lundberg, L.; Mazur, M.; Lorences-Riesgo, A.; Karlsson, M.; Andrekson, P.A. Joint Carrier Recovery for DSP Complexity Reduction in Frequency Comb-Based Superchannel Transceivers. In Proceedings of the European Conference on Optical Communication (ECOC), Gothenburg, Sweden, 17–21 September 2017; p. Th.1.D.3.
67. Mazur, M.; Lorences-Riesgo, A.; Schröder, J.; Andrekson, P.; Karlsson, M. High Spectral Efficiency PM-128QAM Comb-Based Superchannel Transmission Enabled by a Single Shared Optical Pilot Tone. *J. Lightw. Technol.* **2017**, *36*, 1318–1325. [CrossRef]
68. Mazur, M.; Schröder, J.; Lorences-Riesgo, A.; Yoshida, T.; Karlsson, M.; Andrekson, P.A. 11.5bits/s/Hz PM-256QAM Comb-based Superchannel Transmission by Combining Optical and Digital Pilots. In Proceedings of the Optical Fiber Communication Conference (OFC), San Diego, CA, USA, 11–15 March 2018; p. M1G.2.

69. Fontaine, N.; Scott, R.P.; Zhou, L.; Soares, F.M.; Heritage, J.; Yoo, S. Real-time full-field arbitrary optical waveform measurement. *Nat. Photon.* **2010**, *4*, 248. [CrossRef]
70. Fontaine, N. Spectrally-sliced Coherent Receivers for THz Bandwidth Optical Communications. In Proceedings of the European Conference on Optical Communication (ECOC), London, UK, 22–26 September 2013; p. Mo.3.C.1.
71. Alic, N.; Myslivets, E.; Temprana, E.; Kuo, B.P.P.; Radic, S. Nonlinearity Cancellation in Fiber Optic Links Based on Frequency Referenced Carriers. *J. Lightw. Technol.* **2014**, *32*, 2690–2698. [CrossRef]
72. Temprana, E.; Myslivets, E.; Kuo, B.P.; Liu, L.; Ataie, V.; Alic, N.; Radic, S. Overcoming Kerr-induced capacity limit in optical fiber transmission. *Science* **2015**, *348*, 1445–1448. [CrossRef] [PubMed]
73. Chandrasekhar, S.; Liu, X.; Zhu, B.; Peckham, D. Transmission of a 1.2-Tb/s 24-carrier no-guard-interval coherent OFDM superchannel over 7200-km of ultra-large-area fiber. In Proceedings of the European Conference on Optical Communication (ECOC), Vienna, Austria, 20–24 September 2009.
74. Winzer, P.J.; Neilson, D.T. From Scaling Disparities to Integrated Parallelism: A Decathlon for a Decade. *J. Lightw. Technol.* **2017**, *35*, 1099–1115. [CrossRef]
75. Liu, X.; Chandrasekhar, S.; Winzer, P.J. Digital Signal Processing Techniques Enabling Multi-Tb/s Superchannel Transmission: An overview of recent advances in DSP-enabled superchannels. *IEEE Signal Process. Mag.* **2014**, *31*, 16–24. [CrossRef]
76. Raybon, G.; Adamiecki, A.; Cho, J.; Jorge, F.; Konczykowska, A.; Riet, M.; Duval, B.; Dupuy, J.Y.; Fontaine, N.; Winzer, P.J.; et al. 180-GBaud All-ETDM Single-Carrier Polarization Multiplexed QPSK Transmission over 4480 km. In Proceedings of the Optical Fiber Communication Conference (OFC), San Diego, CA, USA, 11–15 March 2018; p. Th4C.3.
77. Going, R.; Lauermann, M.; Maher, R.; Tsai, H.S.; Lu, M.; Kim, N.; Corzine, S.; Studenkov, P.; Summers, J.; Hosseini, A.; et al. Multi-channel InP-based coherent PICs with hybrid integrated SiGe electronics operating up to 100GBd, 32QAM. In Proceedings of the European Conference on Optical Communication (ECOC), Gothenburg, Sweden, 17–21 September 2017.
78. Chandrasekhar, S.; Li, B.; Cho, J.; Chen, X.; Burrows, E.; Raybon, G.; Winzer, P. High-spectral-efficiency transmission of PDM 256-QAM with parallel probabilistic shaping at record rate-reach trade-offs. In Proceedings of the European Conference on Optical Communication (ECOC), Dusseldorf, Germany, 18–22 September 2016, p. Th.3.C.1.
79. Agrawal, G.P. *Fiber-Optic Communication Systems*; John Wiley & Sons: Hoboken, NJ, USA, 2011.
80. Kobayashi, N.; Sato, K.; Namiwaka, M.; Yamamoto, K.; Watanabe, S.; Kita, T.; Yamada, H.; Yamazaki, H. Silicon Photonic Hybrid Ring-Filter External Cavity Wavelength Tunable Lasers. *J. Lightw. Technol.* **2015**, *33*, 1241–1246. [CrossRef]
81. Laperle, C.; Osullivan, M. Advances in high-speed DACs, ADCs, and DSP for optical coherent transceivers. *J. Lightw. Technol.* **2014**, *32*, 629–643. [CrossRef]
82. Millar, D.S.; Maher, R.; Lavery, D.; Koike-Akino, T.; Pajovic, M.; Alvarado, A.; Paskov, M.; Kojima, K.; Parsons, K.; Thomsen, B.C.; et al. Design of a 1 Tb/s Superchannel Coherent Receiver. *J. Lightw. Technol.* **2016**, *34*, 1453–1463. [CrossRef]
83. Maher, R.; Xu, T.; Galdino, L.; Sato, M.; Alvarado, A.; Shi, K.; Savory, S.J.; Thomsen, B.C.; Killey, R.I.; Bayvel, P. Spectrally shaped DP-16QAM super-channel transmission with multi-channel digital back-propagation. *Sci. Rep.* **2015**, *5*, 8214. [CrossRef] [PubMed]
84. Puttnam, B.; Luís, R.; Delgado Mendinueta, J.; Sakaguchi, J.; Klaus, W.; Kamio, Y.; Nakamura, M.; Wada, N.; Awaji, Y.; Kanno, A.; et al. Self-Homodyne Detection in Optical Communication Systems. *Photonics* **2014**, *1*, 110–130. [CrossRef]
85. Nakamura, M.; Kamio, Y.; Lu, G.W.; Miyazaki, T. Ultimate Linewidth-Tolerant 20-Gbps QPSK-Homodyne Transmission using a Spectrum-Sliced ASE Light Source. In Proceedings of the Optical Fiber Communication Conference (OFC), Anaheim, CA, USA, 25–29 March 2007; p. OThD4.
86. Mendinueta, J.M.D.; Puttnam, B.J.; Sakaguchi, J.; Luis, R.S.; Klaus, W.; Awaji, Y.; Wada, N.; Kanno, A.; Kawanishi, T. Energy efficient carrier phase recovery for self-homodyne polarization-multiplexed QPSK. In Proceedings of the OptoElectronics and Communications Conference (OECC), Kyoto, Japan, 30 June–4 July 2013; p. ThR3.5.
87. Luís, R.S.; Puttnam, B.J.; Mendinueta, J.M.D.; Shinada, S.; Nakamura, M.; Kamio, Y.; Wada, N. Digital Self-Homodyne Detection. *IEEE Photon. Technol. Lett.* **2015**, *27*, 608–611. [CrossRef]

88. Le Taillandier de Gabory, E.; Arikawa, M.; Hashimoto, Y.; Ito, T.; Fukuchi, K. A Shared Carrier Reception and Processing Scheme for Compensating Frequency Offset and Phase Noise of Space-Division Multiplexed Signals over Multicore Fibers. In Proceedings of the Optical Fiber Communication Conference (OFC), Anaheim, CA, USA, 17–21 March 2013; p. OM2C.2.
89. Delfyett, P.J.; Gee, S.; Choi, M.T.; Izadpanah, H.; Lee, W.; Ozharar, S.; Quinlan, F.; Yilmaz, T. Optical frequency combs from semiconductor lasers and applications in ultrawideband signal processing and communications. *J. Lightw. Technol.* **2006**, *24*, 2701–2719. [CrossRef]
90. Kemal, J.N.; Pfeifle, J.; Marin-Palomo, P.; Pascual, M.D.G.; Wolf, S.; Smyth, F.; Freude, W.; Koos, C. Multi-wavelength coherent transmission using an optical frequency comb as a local oscillator. *Opt. Exp.* **2016**, *24*, 25432–25445. [CrossRef] [PubMed]
91. Mori, K.; Hamaoka, F.; Horikoshi, K.; Fukutoku, M. Stable WDM-Signal-and-LO-frequency Synchronisation and Transmission Employing Multi-Carrier Light Sources and a Multi-Core Fibre for Coherent Photonic Networks. In Proceedings of the European Conference on Optical Communication (ECOC), Dusseldorf, Germany, 18–22 September 2016; p. Tu.1.C.3.
92. Sakaguchi, J.; Awaji, Y.; Wada, N. Optimal Pilot-Tone-Aided Multi-Core Fiber Transmission Using a Wideband Comb Transmitter. *IEEE Photon. Technol. Lett.* **2017**, *29*, 1245–1248. [CrossRef]
93. Fehenberger, T.; Hanik, N.; Eriksson, T.A.; Johannisson, P.; Karlsson, M. On the impact of carrier phase estimation on phase correlations in coherent fiber transmission. In Proceedings of the Tyrrhenian International Workshop on Digital Communications, Florence, Italy, 22 September 2015.
94. Guiomar, F.P.; Carena, A.; Bosco, G.; Bertignono, L.; Nespola, A.; Poggiolini, P. Nonlinear mitigation on subcarrier-multiplexed PM-16QAM optical systems. *Opt. Exp.* **2017**, *25*, 4298–4311. [CrossRef] [PubMed]
95. Sakaguchi, J.; Kumagai, M.; Li, Y.; Ido, T.; Awaji, Y.; Wada, N. DSP-complexity Reduction of QAM-based Coherent Optical Networks Enabled by Seed Lightwave Distribution. In Proceedings of the Conference on Lasers and Electro-Optics (CLEO), San Jose, CA, USA, 10–15 May 2015; p. SW1M.7.
96. Sakaguchi, J.; Awaji, Y.; Wada, N. Seed Lightwave Distribution over 1600 km for 64QAM-Based Coherent WDM Optical Networks with Low DSP-complexity. In Proceedings of the European Conference on Optical Communication (ECOC), Dusseldorf, Germany, 18–22 September 2016; p. W.4.P1.SC5.12.
97. Cruz, F.C. Optical frequency combs generated by four-wave mixing in optical fibers for astrophysical spectrometer calibration and metrology. *Opt. Express* **2008**, *16*, 13267–13275. [CrossRef] [PubMed]
98. Noé, R. Phase noise-tolerant synchronous QPSK/BPSK baseband-type intradyne receiver concept with feedforward carrier recovery. *J. Lightw. Technol.* **2005**, *23*, 802–808. [CrossRef]
99. Alfredsson, A.; Krishnan, R.; Agrell, E. Joint-Polarization Phase-Noise Estimation and Symbol Detection for Optical Coherent Receivers. *J. Lightw. Technol.* **2016**, *34*, 4394–4405. [CrossRef]
100. Feuer, M.D.; Nelson, L.E.; Zhou, X.; Woodward, S.L.; Isaac, R.; Zhu, B.; Taunay, T.F.; Fishteyn, M.; Fini, J.M.; Yan, M.F. Joint Digital Signal Processing Receivers for Spatial Superchannels. *IEEE Photon. Technol. Lett.* **2012**, *24*, 1957–1960. [CrossRef]
101. Van Uden, R.G.H.; Okonkwo, C.M.; Sleiffer, V.A.J.M.; Kuschnerov, M.; De Waardt, H.; Koonen, A.M.J. Single DPLL joint carrier phase compensation for few-mode fiber transmission. *IEEE Photon. Technol. Lett.* **2013**, *25*, 1381–1384. [CrossRef]
102. Van Uden, R.G.H.; Okonkwo, C.M.; Chen, H.; De Waardt, H.; Koonen, A.M.J. 28-GBd 32QAM FMF transmission with low complexity phase estimators and single DPLL. *IEEE Photon. Technol. Lett.* **2014**, *26*, 765–768. [CrossRef]
103. Liu, C.; Pan, J.; Detwiler, T.; Stark, A.; Hsueh, Y.T.; Chang, G.K.; Ralph, S.E. Joint digital signal processing for superchannel coherent optical communication systems. *Opt. Exp.* **2013**, *21*, 8342–8356. [CrossRef] [PubMed]
104. Souto, D.V.; Olsson, B.E.; Larsson, C.; Mello, D.A.A. Joint-Polarization and Joint-Subchannel Carrier Phase Estimation for 16-QAM Optical Systems. *J. Lightw. Technol.* **2012**, *30*, 3185–3191. [CrossRef]
105. Alfredsson, A.F.; Agrell, E.; Wymeersch, H.; Karlsson, M. Phase-Noise Compensation for Spatial-Division Multiplexed Transmission. In Proceedings of the Optical Fiber Communication Conference (OFC), Los Angeles, CA, USA, 19–23 March 2017; p. Th4C.7.
106. Alfredsson, A.F.; Agrell, E.; Wymeersch, H.; Karlsson, M. Pilot Distributions for Phase Tracking in Space-Division Multiplexed Systems. In Proceedings of the European Conference on Optical Communication (ECOC), Gothenburg, Sweden, 17–21 September 2017, p. P1.SC3.48.

107. Savory, S.J. Digital Coherent Optical Receivers: Algorithms and Subsystems. *IEEE J. Sel. Top. Quantum Electron.* **2010**, *16*, 1164–1179. [CrossRef]
108. Pfau, T.; Hoffmann, S.; Noé, R. Hardware-Efficient Coherent Digital Receiver Concept With Feedforward Carrier Recovery for M-QAM Constellations. *J. Lightw. Technol.* **2009**, *27*, 989–999. [CrossRef]
109. Proakis, J.G.; Salehi, M. *Digital Communications*, 5th ed.; McGraw-Hill Higher Education: New York, NY, USA, 2008.
110. Slavik, R.; Farwell, S.G.; Wale, M.J.; Richardson, D.J. Compact Optical Comb Generator Using InP Tunable Laser and Push-Pull Modulator. *IEEE Photon. Technol. Lett.* **2015**, *27*, 217–220. [CrossRef]
111. Zanette, K.; Cartledge, J.C.; O'Sullivan, M. Correlation properties of the phase noise between pairs of lines in a quantum-dot optical frequency comb source. In Proceedings of the Optical Fiber Communication Conference (OFC), Los Angeles, CA, USA, 19–23 March 2017; p. Th3I.6.
112. Zanette, K.; Cartledge, J.C.; Hui, R.; O'Sullivan, M. Phase Noise Characterization of a Mode-Locked Quantum-Dot Coherent Optical Frequency Comb Source Laser. In Proceedings of the Optical Fiber Communication Conference (OFC), San Diego, CA, USA, 11–15 March 2018; p. Th2A.17.